Insoluble Aβ overexpression in an *App* knock-in mouse model alters microstructure and gamma oscillations in the prefrontal cortex, and social and anxiety-related behaviours

Eleftheria Pervolaraki[1], Stephen P Hall[2], Denise Foresteire[3], Takashi Saito[4], Takaomi C Saido[4], Miles A Whittington[2], Colin Lever[3], James Dachtler[3]

[1]School of Biomedical Sciences, University of Leeds, LS2 9JT, UK

[2]Hull York Medical School, University of York, Heslington, YO10 5DD, UK

[3]Department of Psychology, Durham University, South Road, Durham, DH1 3LE, UK

[4]Laboratory for Proteolytic Neuroscience, RIKEN Brain Science Institute, Wako-shi, Saitama, Japan.

Address for Correspondence: Dr J Dachtler, Department of Psychology, Durham University, Durham, DH1 3LE, UK. James.dachtler@durham.ac.uk

Abstract

We studied two new *App* knock-in mice models of Alzheimer's disease (*App*$^{NL-F}$ and *App*$^{NL-G-F}$), which generate elevated levels of $A\beta_{40}$ and $A\beta_{42}$ without the confounds associated with APP overexpression. This enabled us to assess changes in anxiety-related and social behaviours, and neural alterations potentially underlying such changes, driven specifically by Aβ accumulation. *App*$^{NL-G-F}$ knock-in mice exhibited subtle deficits in tasks assessing social memory, but not in social motivation tasks. In anxiety-assessing tasks, *App*$^{NL-G-F}$ knock-in mice exhibited: 1) increased thigmotaxis in the Open Field (OF), yet; 2) reduced closed-arm, and increased open-arm, time in the Elevated Plus Maze (EPM). Their ostensibly-anxiogenic OF profile, yet ostensibly-anxiolytic EPM profile, could hint at altered cortical mechanisms affecting decision-making (e.g. 'disinhibition'), rather than simple core deficits in emotional motivation. Consistent with this possibility, alterations in microstructure, glutamatergic-dependent gamma oscillations, and glutamatergic gene expression were all observed in the prefrontal cortex, but not the amygdala, of *App*$^{NL-G-F}$ knock-in mice. Thus, insoluble Aβ overexpression drives prefrontal cortical alterations, potentially underlying changes in social and anxiety-related behavioural tasks.

Key words:

Alzheimer's disease; App^{NL-G-F} knock-in mice, anxiety, prefrontal cortex, gamma oscillations, social

Highlights

- *App*$^{NL-G-F}$ KI mice displayed differing anxiety behaviours in two tests of anxiety.

- Prefrontal gamma was no longer NMDA-receptor dependent in *App*$^{NL-G-F}$ KI mice.
- Prefrontal expression of *Grin2b* was reduced in *App*$^{NL-G-F}$ KI mice.
- DTI found structural alterations in the hippocampus and prefrontal cortex in *App*$^{NL-G-F}$ KI mice.

Abbreviations

DTI: diffusion tensor MRI; FA: fractional anisotropy; MD: mean diffusivity; AD: axial diffusivity; RD: radial diffusivity; Aβ: amyloid beta; KI: knock-in; APP: amyloid precursor protein

Disclosure

The authors have no actual or potential conflicts of interest.

Acknowledgements

This work was supported an Alzheimer's Society (UK) Fellowship (AS-JF-15-008) to JD and a Wellcome Trust (UK) grant to MAW.

Introduction

Alzheimer's disease (AD) is classically associated with declining cognitive function (Scheltens, et al., 2016). However, this is only one aspect of the behavioural changes associated with AD. Other behavioural changes include reduced social engagement and increased anxiety. Although social aspects of AD have remained underexplored, social withdrawal is present up to 5 years prior to a clinical cognitive diagnosis (Jost and Grossberg, 1995). AD patients with larger social networks (the number of people with which one has meaningful contact with) have slower cognitive decline, compared to AD patients with small social networks (Bennett, et al., 2006). Social factors may modulate the rate of disease pathology and cognitive decline, but crucially, also the chance of developing AD (Kuiper, et al., 2015). Studies have found that for the elderly that identify as lonely, the risk of developing AD was nearly doubled (Wilson, et al., 2007). Recent evidence from the Lancet Commission Report highlights that social isolation constitutes a 2.3% risk of developing AD (Livingston, et al., 2017). Thus, social factors not only modulate the risk of developing dementia, but also disease progression. Together, it can be inferred that changes in social motivation of the individual as a result of AD pathology may be a factor in disease progression.

Anxiety in AD is relatively common, with up to 71% of patients reporting anxiety concerns (Ferretti, et al., 2001,Teri, et al., 1999). Up to 6% had anxiety that reached the diagnostic criteria of generalised anxiety disorder of Diagnostic and Statistical Manual of Mental Disorders (Ferretti, et al., 2001). Anxiety behaviours may also predict conversion to AD. Mild cognitive impairment (MCI) is thought to be a precursor condition to AD. 83.3% of MCI patients that also exhibited anxiety

symptoms converted to AD within a three year follow up period compared to 40.9% of persons with MCI but without anxiety (Palmer, et al., 2007). The latter suggests that anxiety is associated with early phases of AD. Neurodegeneration in brain structures in early AD may explain the increase in anxiety. Extensive literature has linked the amygdala to anxiety behaviours (Shin and Liberzon, 2010). In very mild and mild AD, amygdala atrophy was similar to that of the hippocampus and was correlated to anxiety (Poulin, et al., 2011), suggesting that amygdala degeneration could explain AD-related anxiety. Together, non-cognitive behavioural changes in AD can occur early in disease progression and have clear modulatory effects on disease progression. Currently, we have few insights into the biological mechanisms underpinning anxiety and social withdrawal in AD, highlighting the need to find AD mice that model these behaviours.

Broadly speaking, pathologies underpinning AD tend to group into two domains; those of amylogenic pathways and those of tau, although the two are not mutually exclusively (Bloom, 2014). The animal models have tended to focus on only one of these pathology pathways, although the majority of these model the amyloid aspects of AD through amyloid-β peptide (Aβ) plaques. Despite many transgenic mouse models of AD existing, previous generations of Aβ mice have achieved their Aβ overexpression by also overexpressing amyloid precursor protein (APP). Over time, it has become clear the APP overexpression alone can introduce confounds that make it difficult to dissociate the causal effects of Aβ compared to APP. Mice overexpressing human wild-type APP have cognitive impairments in the Morris watermaze and object recognition test, increased tau hyperphosphorylation and reduced GluA1, GluA2, GluN1, GluN2A, GluN2B, phosphorylated CaMKII and

PSD95 (Simon, et al., 2009). This was also associated with reduced cell density in the pyramidal layer of CA1 (Simon, et al., 2009). Others have found that other Aβ mice (the APP23) produced higher amounts of APP fragments, including C-terminal fragment β/α and APP intracellular domain (Saito, et al., 2014). The phenotypes associated with APP overexpression alone encapsulate what are known to be AD-specific pathologies, underlining the potential risks of using APP overexpression models to make AD interpretations.

Recently, a new generation of AD mouse models have become available that achieves Aβ pathologies without the overexpression of APP (Saito, et al., 2014). This has been achieved by humanising the murine Aβ sequence through a knock-in (KI) strategy. Up to three familial mutations have been knocked-in to generate two AD mouse models. The *App*$^{NL-F}$ mouse contains the Swedish KM670/671NL mutation and the Iberian I716F mutation which results in elevated total Aβ and elevated $A\beta_{42}/A\beta_{40}$ ratio (Saito, et al., 2014). The *App*$^{NL-G-F}$ mouse also contains the Swedish and Iberian mutations, but with the additional Artic mutation E693G which promotes aggressive Aβ oligomerisation and amyloidosis (Saito, et al., 2014). In *App*$^{NL-G-F}$ mice, Aβ plaques are saturated by 9 months of age, but by contrast, *App*$^{NL-F}$ mice exhibit relatively few plaques. Both models have approximately similar amounts of soluble Aβ species (Saito, et al., 2014). Hence, these two mouse models are useful to be able to dissociate the effects of soluble Aβ and plaque-based Aβ in the generation of AD-related pathologies.

Within the current study, we have sought to explore whether these new *App* KI mouse models display alterations in behaviours related to social motivation, social

memory and anxiety. We subsequently used electrophysiology, diffusion tensor MRI (DTI) and quantitative PCR (qPCR) to determine putative biological mechanisms that may explain, with brain region specificity, the underlying cause of behavioural impairments.

Materials and Methods

Ethics

All procedures were approved by the Durham University and University of York Animal Ethical and Welfare Review Boards and were performed under UK Home Office Project and Personal Licenses in accordance with the Animals (Scientific Procedures) Act 1986.

Mice

Full details of the animals can be found elsewhere (Saito, et al., 2014). Upon arrival at Durham, mice were backcrossed once to the C57BL/6J line, which was the same background strain as the previous institution where they were bred. Homozygote App^{NL-F} and App^{NL-G-F} and wild-type littermate mice were bred in house by heterozygote pairings and were weaned at P21 and ear biopsied for genotyping. Genotyping protocols can be found elsewhere (Saito, et al., 2014). All mice were housed with littermates.

Experimental animals

Behaviour

21 wild-type (9 male (8.19 months ± 0.12), 11 female (8.10 months ± 0.04)), 19 App^{NL-F} homozygotes (10 male (7.83 months ± 0.15), 9 female (7.64 months ± 0.14)) and 19 App^{NL-G-F} homozygotes (10 male (7.93 months ± 0.17), 9 female (7.44 months ± 0.43)) were used in behavioural testing. Mice were transferred to the testing room and allowed at least 30 mins habituation prior to testing. All mice were transferred to the apparatus via cardboard tubes.

Testing procedures can be found elsewhere (Dachtler, et al., 2014). All trials were recorded by Any-maze (Stoelting, Dublin, Ireland) tracking software. Mice undertook the following test in this order: open field, elevated plus maze, social approach, social recognition and social olfactory discrimination. In brief, mice were placed into a 44 cm^2 white Perspex arena and allowed free ambulation for 30 mins. The floor of the arena was divided by Any-maze into an outer zone of 8 cm and a centre zone of 17.5 cm^2. Time spent and entries into these zones, along with distance travelled were measured. The elevated plus maze and social approach, social recognition, and social olfaction discrimination was run as in (Dachtler, et al., 2014), except that novel conspecifics and soiled bedding was sex matched with adult mice to the test subject. At the conclusion of testing, mice were either used for electrophysiology, killed by perfusion fixation with 4% paraformaldehyde in phosphate buffered saline (PBS) or killed by cervical dislocation for molecular biology.

Diffusion Tensor MRI

8 wild-type (4 male (9.02 months ± 0.63), 4 female (9.43 months ± 0.30)) and 8 *App*$^{NL-G-F}$ homozygotes (4 male (8.88 months ± 0.22), 4 female (9.89 months ± 0.21)) were used in for MR imaging. Image acquisition has been described elsewhere (Pervolaraki, et al., 2017). MR imaging was performed on a vertical 9.4 Tesla spectrometer (Bruker AVANCE II NMR, Ettlingen, Germany). During imaging, the samples were placed in custom-built MR-compatible tubes containing Fomblin Y (Sigma, Poole, Dorset, UK). The following acquisition protocol was used: TE: 35 ms, TR: 700 ms, 1 signal average. The field of view was set at 168 x 128 x 96, with a cubic resolution of 62.5 µm/pixel and a B value of 1625 s/mm with 30 directions.

The *ex vivo* mouse brain 3D diffusion-weighted images were reconstructed from the Bruker binary file using DSI Studio (http://dsi-studio.labsolver.org). Direction Encoded Colour Map (DEC) images were generated by combining the information from the primary eigenvectors, diffusion images and the fractional anisotropy (FA). Regions were extracted by manually segmenting orbitofrontal cortex (OFC), anterior cingulate cortex (ACC), hippocampal and whole amygdalar regions using a mouse brain atlas (Franklin and Paxinos, 2008). We chose to focus on the aforementioned brain regions as these have been linked to social behaviour (Eleftheria Pervolaraki, et al., 2018). Additionally, the hippocampus (Bannerman, et al., 2004,McHugh, et al., 2004), the amygdala (Davis, 1992,Davis, et al., 1994) and prefrontal cortical regions (including the ACC) (Davidson, 2002,Etkin, et al., 2011) have all been linked to anxiety. Extraction of FA, mean diffusivity (MD), axial diffusivity (AD) and radial diffusivity (RD) was performed within selected segmented brain regions, with 3 100 µm sections (one anterior and one posterior to the segmented section) extracted. Full atlas-based description of the segmentation can be found in Pervolaraki et al. (2018).

Electrophysiology

Anterior cingulate or basolateral amygdala coronal slices (450 µm thick) were prepared from age-matched, 12 month old male wild-type (n=5) mice and *App*$^{NL\text{-}G\text{-}F}$ KI (n=5) mice. Animals were anesthetised with inhaled isoflurane, immediately followed by an intramuscular injection of ketamine (100 mg/kg) and xylazine (10 mg/kg). Animals were perfused intracardially with 50-100ml of modified artificial cerebrospinal fluid (ACSF), which was composed of the following (in mM): 252 sucrose, 3 KCl, 1.25 NaH_2PO_4, 24 $NaHCO_3$, 2 $MgSO_4$, 2 $CaCl_2$, and 10 glucose. The

brain was removed and submerged in cold (4–5°C) ACSF during dissection. Once dissected, slices were maintained at 32°C in a standard interface recording chamber containing oxygenated ACSF consisting of (in mM): 126 NaCl, 3 KCl, 1.25 NaH_2PO_4, 1 $MgSO_4$, 1.2 $CaCl_2$, 24 $NaHCO_3$ and 10 glucose. Persistent, spontaneous gamma oscillations were generated through the bath application of 400 nM kainic acid (KA). Further perfusion, through bath application of 20 mM 3-(2-Carboxypiperazin-4-yl)propyl-1-phosphonic acid (CPP), was conducted to antagonise NMDA receptors. All salts were obtained from BDH Chemicals (Poole, UK) or Sigma-Aldrich (Poole, UK) and KA and CPP were obtained from BioTechne (Minnesota, USA).

Extracellular field recordings were obtained using borosilicate micropipettes (Harvard Apparatus) filled with ACSF and had resistances of 2-5 (MΩ). Recordings were bandpass filtered at 0.1Hz to 300Hz. Power spectra were derived from Fourier transform analysis of 60 s epochs of data and results were presented as mean ± SEM.

RNA Extraction and qPCR

For molecular biology, mice underwent cervical dislocation, with the brain extracted and placed into a mouse brain blocker (David Kopf Instruments, Tujunga, USA). The olfactory bulbs were removed, followed by a section of tissue from Bregma 3.56 to 2.58 mm, and from Bregma -0.82 to -2.80 mm. The tissue containing prefrontal tissue was snap frozen. The posterior section was then further dissected with a scalpel to remove the amygdalar region, which was then snap frozen and stored at -80°C until use. 6 wild-type (4 male, 2 female (10.26 months ± 0.41)) and 6 App^{NL-G-F} homozygotes (3 male, 3 female (9.49 months ± 0.13)) were used for qPCR. Brain

tissue of extracted regions (amygdala and prefrontal cortex) were homogenised by TissueRuptor drill (Qiagen, Manchester, UK), with ~90 mg used for RNA extraction. Instructions were followed as per the Bio-Rad Aurum Total RNA Fatty and Fibrous Tissue Kit (Bio-Rad, Hemel Hempsted, UK, Cat# 7326830) and our previously optimised protocol (E. Pervolaraki, et al., 2018). RNA quantity and quality were confirmed by Nanodrop spectrophotometer. cDNA was generated by the iScript cDNA Synthesis Kit (Bio-Rad, UK), with 1 µg of RNA used per reaction.

Primers (Table 1) were designed using Primer3 after identifying the gene sequence on NCBI. Primers (Integrated DNA Technologies, Leuven, Belgium) were tested for specificity and run conditions optimised by PCR using whole brain cDNA. Plates were run with 10 µl per reaction, with 1 µl of cDNA, Bio-Rad SYBR Green (cat# 1725121) and 300 nM primers. Samples were run in triplicate using the protocol of 95C for 3 min, followed by 95C for 10 s, 60C for 30 s repeated 35 times. Gene expression was imaged using a Bio-Rad CFX Connect and analysed using Bio-Rad Connect Manager, and quantified using the 2^ddCt method against the housekeeping gene *Gapdh* which did not differ between the genotypes.

Immunostaining

Staining for amyloid plaques can be found elsewhere (Ly, et al., 2011). Tissue previously scanned by MRI was washed and immersed in 30% sucrose for >48 hrs. Tissue was cryosectioned at 30 µm, followed by immersion in 88% formic acid for 15 mins. Endogenous peroxidase activity was quenched with H_2O_2 for 30 mins, followed by blocking in 2% bovine serum albumin (BSA) (Thermo Fisher Scientific) for 1 hr at room temperature. Sections were then incubated with 1:500 6E10 (BioLegend, San

Diego, CA, USA) overnight at 4°C, followed by 1:500 biotinylated anti-mouse (Vector Labs, Peterborough, UK) for 2 hrs at room temperature. Sections were then reacted with Vectastain ABC kit (Vector Labs) followed by diaminobenzidine (DAB) treatment (Vector Labs) prior to mounting on slides for imaging by light microscopy.

Data Analysis

All data are expressed as mean ± standard error of the mean (SEM). To assess the variance between genotypes within a single brain structure across hemispheres, data was analysed by within subject repeated measures two-way ANOVAs or unpaired T-tests. To correct for multiple comparisons, we employed the Benjamini-Hochberg Procedure, with false discovery rate set to 0.4 (corrected P values stated). Behaviour was analysed with ANOVAs, followed by tests of simple main effects. To test for discrimination against chance, one sample T-tests were used set against chance (0.5). Non-significant statistical results, particularly hemisphere comparisons, can be found in Supplemental Materials. Statistical testing and graphs were made using GraphPad Prism version 6 and SPSS v22.

Results

App^{NL-G-F} KI mice have changes in emotional behaviours

To assess the potential role of Aβ in emotional behaviour, we undertook two behavioural paradigms that are widely used to probe anxiety: the open field and the elevated plus maze. In the open field, mice were allowed to freely ambulate for 30 mins, during which we measured the distance they travelled in 5 min blocks. We observed that both *App*$^{NL-F}$ and *App*$^{NL-G-F}$ KI mice travelled a similar distance to wild-type mice (Fig. 1A; genotype $F_{(2, 55)} = 2.19$, $p = 0.122$, time block x genotype x sex $F_{(1, 55)} < 1$, $p = 0.817$, genotype x sex $F_{(2, 55)} = 1.21$, $p = 0.306$), suggesting that *App* KI mice do not have any overt deficiencies in motor function. We subsequently divided the floor of the arena into an outer zone and a centre zone (see Methods) to determine whether *App* KI mice displayed a propensity to stay close to the walls (thigmotaxis) and avoid the centre. Whilst wild-type and *App*$^{NL-F}$ KI mice spend a broadly similar amount of time in the outer zone, *App*$^{NL-G-F}$ KI mice spend significantly more time against the walls (Fig. 1B; genotype $F_{(2, 55)} = 10.34$, $p < 0.0001$, genotype x sex $F_{(2, 55)} < 1$, $p = 0.475$. Tukey's post hoc: wild-type vs. *App*$^{NL-G-F}$ KI mice $p = 0.001$, *App*$^{NL-F}$ KI mice vs. *App*$^{NL-G-F}$ KI mice $p = 0.001$). We next examined whether *App* KI mice spent less time exploring the centre zone, which would further confirm an anxiogenic phenotype. Similar to the outer zone, we found that *App*$^{NL-G-F}$ KI mice spent significantly less time in the centre zone (Fig. 1C; genotype $F_{(2, 55)} = 7.49$, $p = 0.001$, genotype x sex $F_{(2, 55)} < 1$, $p = 0.603$. Tukey's post hoc: wild-type vs. *App*$^{NL-G-F}$ KI mice $p = 0.003$, *App*$^{NL-F}$ KI mice vs. *App*$^{NL-G-F}$ KI mice $p = 0.006$). Although *App*$^{NL-G-F}$ KI mice show an anxiety phenotype as shown by time spent in the centre and outer zones, no differences between the genotypes were observed for entries to the outer zone or the centre zone (Supplementary Fig. 1A,

1B, see figure legend for statistics), suggesting that all genotypes explored the arena similarly.

We next examined whether *App*$^{NL\text{-}G\text{-}F}$ KI mice also had a similar anxiogenic profile in the elevated plus maze. Surprisingly, *App*$^{NL\text{-}G\text{-}F}$ KI mice spent significantly more time in the open arms of the elevated plus maze (Fig. 1D; genotype $F_{(2, 55)} = 4.25$, $p = 0.019$, sex $F_{(1, 55)} < 1$, $p = 0.806$, genotype x sex $F_{(2, 55)} = 1.52$, $p = 0.229$. Tukey's post hoc: wild-type vs. *App*$^{NL\text{-}G\text{-}F}$ KI mice $p = 0.032$, *App*$^{NL\text{-}F}$ KI mice vs. *App*$^{NL\text{-}G\text{-}F}$ KI mice $p = 0.067$). Conversely, *App*$^{NL\text{-}G\text{-}F}$ KI mice spent significantly less time in the closed arm (Fig. 1E; genotype $F_{(2, 55)} = 8.69$, $p = 0.001$, sex $F_{(1, 55)} < 1$, $p = 0.664$, genotype x sex $F_{(1, 55)} = 1.69$, $p = 0.195$. Tukey's post hoc: wild-type vs. *App*$^{NL\text{-}G\text{-}F}$ KI mice $p = 0.005$, *App*$^{NL\text{-}F}$ KI mice vs. *App*$^{NL\text{-}G\text{-}F}$ KI mice $p = 0.001$). Furthermore, *App*$^{NL\text{-}G\text{-}F}$ KI mice spent significant more time in the centre zone compared to *App*$^{NL\text{-}F}$ KI mice but not wild-types (see Supplementary Fig. 1C for statistics), and there were trends towards significantly more head dips made by *App*$^{NL\text{-}G\text{-}F}$ KI mice from the centre zone (see Supplementary Fig. 1D for statistics). The specificity of differences are unlikely to be explained by hyper or hypoactivity, as all genotypes travelled a similar distance within the test (see Supplementary Fig. 1E for statistics). In summary, *App*$^{NL\text{-}G\text{-}F}$ KI mice have alterations in their anxiety profile that differ between experimental paradigms.

To explore whether social motivation was altered in *App* KI mice, we examined sociability in the three-chambered social approach test (Moy, et al., 2004,Nadler, et al., 2004) which exploits the preference of a mouse to explore a novel mouse enclosed within a wire cage compared to an identical empty cage. All genotypes

showed clear preference for exploring the cage containing the novel mouse, and this did not differ between the genotypes (Fig. 2A: genotype $F_{(2, 55)} = 1.71$, $p = 0.19$, genotype x discrimination $F_{(2, 55)} < 1$, $p = 0.576$, genotype x sex $F_{(1, 55)} = 1.98$, $p = 0.149$). Next, we tested whether *App* KI mice were able to show social novelty preference for exploring a second novel conspecific compared to the previous explored conspecific (Fig. 2B). We found a significant interaction between genotype and sex for social novelty recognition ($F_{(2, 55)} = 3.39$, $p = 0.041$), although there was no main effect of genotype ($F_{(2, 55)} = 2.31$, $p = 0.11$) or genotype x discrimination ($F_{(1, 55)} = 1.17$, $p = 0.32$).

To further explore this sex effect, we specifically examined whether the discrimination ratios for social novelty preference for each genotypic sex were above chance. For both males (Fig. 2C) and females (Fig. 2D), only wild-type mice displayed discrimination that was significantly above chance, with male App^{NL-F} and App^{NL-G-F} KI mice showing greater variation in performance (see Fig. 2 legend for statistics).

Finally, we tested whether *App* KI mice showed motivation to explore a social smell (soiled bedding) compared to a non-social smell (clean bedding). Similar to the social novelty preference, we observed that discrimination between the social and non-social olfactory stimulus differed by sex and genotype (Supplementary Fig. 2: genotype x discrimination x sex $F_{(2, 55)} = 4.31$, $p = 0.019$, genotype x discrimination $F_{(2, 55)} < 1$, $p = 0.619$, genotype x sex $F_{(1, 55)} = 2.01$, $p = 0.144$). To further investigate the source of difference, we examined the discrimination ratios separated by sex (Fig. 2E,F). For males, all genotypes show significant preference for exploring the

social smell compared to chance. However, although female wild-type and *App*$^{NL-F}$ KI mice showed preference for the social smell, female *App*$^{NL-G-F}$ KI mice were not significantly different from chance (see Figure legend for statistics).

App^{NL-G-F} KI mice have microstructural changes in the prefrontal cortex and hippocampus

Given that behavioural changes in the open field, elevated plus maze and social olfaction test are altered only in *App*$^{NL-G-F}$ KI mice, we decided to take this genotype forward for further analysis to determine the biological mechanisms that may explain these impairments. Our approach was to examine the integrity of brain regions associated with both social and anxiety behaviours (see Methods). These centred upon the prefrontal cortex (OFC and ACC), the hippocampus (anterior and posterior) and the amygdala (including the basolateral (BLA)). To derive quantitative measures of DTI, we examined FA and MD (examining diffusion across the λ_1, λ_2 and λ_3 vectors), followed by AD and RD (to determine preferential diffusion along the λ_1, or λ_2 and λ_3 vectors, respectively).

Given the amygdala has been widely associated with both social and anxiety behaviours (Adolphs, 2010,Davis, 1992,Davis, et al., 1994), we segmented the whole amgdalar region, in anterior and posterior planes, and separately, the basolateral nuclei (BLA), to determine whether structural alterations may explain the behavioural changes. For all measures (FA, MD, AD and RD), in both the anterior and posterior amygdala, plus the BLA, we did not observe any significant changes in tissue diffusion properties (Supplementary Table 1 for non-significant statistics and Supplementary Fig. 3).

Ventral hippocampal regions have been associated with anxiety and fear behaviours (Bannerman, et al., 2004), whilst dorsal and ventral regions are increasingly being associated with social recognition (Hitti and Siegelbaum, 2014,Okuyama, et al., 2016). We therefore next examined the microstructure of the hippocampus along the anterior to posterior axis. FA of the anterior (Fig. 3A) and posterior (Fig. 3B) hippocampus did not differ between wild-types (Supplementary Table 2 for non-significant statistics). However, whilst MD in the anterior hippocampus (Fig. 3C) was similar between the genotypes $F_{(1, 14)} < 1$, $p = 0.263$), MD was significantly higher in the posterior hippocampus (Fig. 3D) in *App*$^{NL\text{-}G\text{-}F}$ KI mice ($F_{(1, 14)} = 12.18$, $p = 0.011$). For AD, *App*$^{NL\text{-}G\text{-}F}$ KI mice had significantly increased diffusion in the anterior hippocampus (Fig. 3E $F_{(1, 14)} = 7.55$, $p = 0.047$) but not in the posterior hippocampus (Fig. 3F $F_{(1, 14)} = 4.45$, $p = 0.068$). RD was significantly higher in *App*$^{NL\text{-}G\text{-}F}$ KI mice in the posterior hippocampus (Fig. 3G $F_{(1, 14)} = 18.13$, $p = 0.005$) but not the anterior hippocampus (Fig. 3H $F_{(1, 14)} = 1.52$, $p = 0.142$).

We next segmented prefrontal cortical regions including the OFC and the ACC. In addition to roles for OFC and ACC regions in anxiety and social behaviours, resting state functional MRI (rsfMRI) has shown that the ACC was the most altered brain region in *App*$^{NL\text{-}G\text{-}F}$ KI mice. However, it is currently unknown as to whether structural changes in the ACC contributed to the rsfMRI result. In the OFC of *App*$^{NL\text{-}G\text{-}F}$ KI mice, there were no significant differences in FA (Fig. 4A; genotype ($F_{(1, 14)} = 4.51$, $p = 0.063$), however MD was significantly increased (Fig. 4B; genotype ($F_{(1, 14)} = 8.61$, $p = 0.026$). Similarly, for the ACC, FA was similar between the genotypes (Fig. 4C; genotype ($t_{(14)} < 1$, $p = 0.37$) but MD was significantly increased (Fig. 4D; genotype

($t_{(14)}$ = 3.13, p = 0.021). We furthered explored prefrontal cortical changes by quantifying AD and RD. In the OFC, both AD and RD were significantly increased in *App*$^{NL\text{-}G\text{-}F}$ KI mice ($F_{(1, 14)}$ = 8.34, p = 0.032 (Fig. 4E) and $F_{(1, 14)}$ = 8.23, p = 0.042 (Fig. 4F), respectively). AD and RD were also significantly increased in the ACC of *App*$^{NL\text{-}G\text{-}F}$ KI mice ($t_{(14)}$ = 2.88, p = 0.037 (Fig. 4G) and $t_{(14)}$ = 3.19, p = 0.016 (Fig. 4H). Finally, we performed amyloid plaque staining on corresponding tissue sections as was analysed for DTI. By 9 months of age in *App*$^{NL\text{-}G\text{-}F}$ KI mice, the OFC, ACC, amygdala and hippocampus all exhibit substantial plaque load (Supplementary Fig. 4), indicating that the lack of DTI changes in the amygdala are not due to an absence of amyloid plaques.

Alterations in prefrontal cortical NMDA-dependent gamma oscillations in *App*$^{NL\text{-}G\text{-}F}$ KI mice

Although some microstructure changes were detected in the hippocampus of *App*$^{NL\text{-}G\text{-}F}$ KI mice (anterior hippocampal AD and posterior hippocampal RD), these were relatively inconsistent compared to the alterations observed within the prefrontal cortex. Another study found the ACC as being the most significantly altered brain region in *App*$^{NL\text{-}G\text{-}F}$ KI mice as detected by rsfMRI (Latif-Hernandez, et al., 2017), suggesting that substantial changes are occurring in the ACC. As such, and given the purported importance of the ACC and amygdala to anxiety and social behaviours, we decided to contrast these two regions to examine whether prefrontal function is affected as a result of the DTI-derived microstructural alterations.

Gamma oscillations have been widely associated with roles in learning, coherence between brain regions facilitating information transfer (Buzsaki and Wang, 2012),

social behaviour (Cao, et al., 2018) and anxiety behaviours within the medial prefrontal cortex (Adhikari, et al., 2010). Gamma has been shown to disrupted in other AD mouse models, such as the APP/PS1 (Klein, et al., 2016), the TAS10 overexpression model (Driver, et al., 2007) and in the entorhinal cortex of *App*$^{NL-G-F}$ KI mice (Nakazono, et al., 2017), and these impairments occur relatively early into Aβ pathology. Thus, gamma oscillations represent a useful target for exploring AD-related pathology.

We generated gamma oscillations in brain slices using kainate and tested their dependency on NMDA receptors, which have previously been shown to modulate peak frequency through inhibitory postsynaptic currents (McNally, et al., 2011) by modifying recruitment of different interneuron subpopulations (Middleton, et al., 2008). Within the BLA of the amygdala, we found that in wild-types, peak amplitude and frequency of gamma oscillations were unaffected by the application of the broad spectrum antagonist NMDA receptor antagonist CPP (Fig. 5Aiii; $t_{(14)}$ <1, p = 0.991 and $t_{(14)}$ <1, p = 0.656, respectively). We observed similar results in the *App*$^{NL-G-F}$ KI mice with peak amplitude and frequency unaffected by NMDA antagonism (Fig. 5Aiv; $t_{(14)}$ <1, p = 0.951 and $t_{(14)}$ <1, p = 0.709, respectively). Together, this suggests that gamma oscillations in the BLA in *App*$^{NL-G-F}$ KI mice are unaffected by Aβ deposition.

Next, we studied gamma oscillations within the ACC of the prefrontal cortex. In wild-types, the frequency of gamma oscillations were unaffected by CPP (Fig. 5Biii; $t_{(14)}$ = 1.91, p = 0.086). However, gamma peak amplitude was significantly reduced by CPP application (Fig. 5Biv; $t_{(14)}$ = 2.96, p = 0.014), suggesting that ACC gamma oscillations require NMDA receptors. In *App*$^{NL-G-F}$ KI mice, we found that unlike in

wild-types, neither gamma frequency nor amplitude was altered by NMDA receptor antagonism ($t_{(14)}$ <1, p = 0.430 and $t_{(14)}$ <1, p = 0.404, respectively), suggesting that ACC gamma oscillations in *App*$^{NL-G-F}$ KI mice have lost their dependency upon NMDA receptors.

To further analyse the NMDA receptor-dependent alterations in the prefrontal cortex, we next analysed the mRNA expression of synaptic genes including NMDA receptors and pre and postsynaptic receptors relating to NMDA receptor function. Within the amygdala, although we generally observed higher gene expression in *App*$^{NL-G-F}$ KI mice (Fig. 6A), no significant genotypic differences were observed for *Dlg4* ($t_{(10)}$ = 2.14, p = 0.058), *Grin1* ($t_{(10)}$ = 1.97, p = 0.078), *Grin2a* ($t_{(10)}$ = 2.16, p = 0.056), *Grin2b* ($t_{(10)}$ <1, p = 0.455) or *Stxbp1* ($t_{(10)}$ = 1.27, p = 0.234). We next examined the mRNA expression in the frontal cortex (Fig. 6B). We did not observed any significant differences between wild-types and *App*$^{NL-G-F}$ KI mice for the genes *Dlg4* ($t_{(10)}$ <1, p = 0.420), *Grin1* ($t_{(10)}$ <1, p = 0.780), and *Grin2a* ($t_{(10)}$ <1, p = 0.731). However, the expression of *Grin2b* ($t_{(10)}$ = 2.59, p = 0.027) and *Stxbp1* (protein: Munc18-1) ($t_{(10)}$ = 2.66, p = 0.024) was significantly reduced in *App*$^{NL-G-F}$ KI mice. Together, the change in the dependency of NMDA receptor mediated gamma in the ACC of *App*$^{NL-G-F}$ KI mice could be related to reduced *Grin2b* or presynaptic release through Munc18-1.

Discussion

Within the current study, we have further characterised the behavioural profile of the new generation of *App* KI mice. Our results indicate that *App*$^{NL-G-F}$ KI mice have differing anxiety behaviours depending upon the paradigm used, and a mild impairment in social recognition and social olfactory discrimination. We further characterised the cellular correlates of these impairments, and found that *App*$^{NL-G-F}$ KI mice have structural alterations in the prefrontal cortex, changes to NMDA-receptor dependent gamma oscillations in the ACC, which may relate to a lack of *Grin2b*.

The development of the *App*$^{NL-F}$ KI and *App*$^{NL-G-F}$ KI mice has allowed researchers to dissociate the amyloidogenic effects of Aβ deposition. At around 9 months of age, *App*$^{NL-G-F}$ KI mice have nearly 100 times the amount of insoluble $A\beta_{42}$ compared to *App*$^{NL-F}$ KI mice (Saito, et al., 2014). Thus, at 9 months, *App*$^{NL-G-F}$ KI mice are almost plaque saturated compared to *App*$^{NL-F}$ KI mice, which have few detectable plaques (Saito, et al., 2014). This enables the dissociation between whether soluble or plaque-based $A\beta_{42}$ results in changes to behavioural performance.

Within the current study, we observed a conflicting phenotype between increased thigmotaxis in the open field (anxiogenic) and increased time in the open arms in the elevated plus maze (anxiolytic). Others have examined the anxiety profile in *App*$^{NL-G-F}$ KI mice using the open field and found that 6 month old mice spent more time in the open field centre zone (Latif-Hernandez, et al., 2017). However, others have found no difference in time spent in the centre of an open field for 6 month old *App*$^{NL-G-F}$ KI mice (Whyte, et al., 2018). Latif-Hernandez et al. (2017) and Whyte et al.

(2018) did not specifically quantify thigmotaxis in the open field, limiting comparisons to our study. Interestingly, locomotion within the open field appears to vary by age. Distance travelled in the open field is significantly greater in 6 month old *App*$^{NL-G-F}$ KI mice, whilst at 8 months (the current study) and 10 months of age, there were no significant differences (Latif-Hernandez, et al., 2017,Whyte, et al., 2018), suggesting hyperactivity is only detectable in younger mice.

Like our study, Latif-Hernandez et al. (2017) also used the elevated plus maze to explore anxiety behaviours in *App*$^{NL-G-F}$ KI mice, except they compared to *App*^{NL} KI mice. They found *App*$^{NL-G-F}$ KI mice spent more time in the open arms at 6 months of age (Latif-Hernandez, et al., 2017), which we replicated at 8 months of age. A very recent study has also found that 6-9 month old *App*$^{NL-G-F}$ KI mice spent more time in the elevated plus maze open arms (Sakakibara, et al., 2018). Together, independent studies suggest that *App*$^{NL-G-F}$ KI mice display an anxiolytic profile in the elevated plus maze. The contradiction between our results in the open field and elevated plus maze is curious but not unique. Tg2576 mice also show open field thigmotaxis yet increased time in the elevated plus maze open arms (Lalonde, et al., 2003). It is possible that the increased time spent in the open arms reflects a disinhibition phenotype. Disinhibition is a well-established, albeit less common, AD phenotype (Chung and Cummings, 2000,Hart, et al., 2003), which could be manifested within the current study as a failure to inhibit the choice to enter the open arm. Given the lack of specific data to speak to a disinhibition hypothesis, it is clear that future anxiety testing in *App*$^{NL-G-F}$ KI mice will require multiple paradigms to clearly delineate anxiety from disinhibition. A benefit of our study is that we are the first to behaviourally compare *App*$^{NL-F}$ KI and *App*$^{NL-G-F}$ KI mice beyond the original Saito

(2014) paper. Regarding the open field and elevated plus maze, genotypic differences were only found in *App*$^{NL\text{-}G\text{-}F}$ KI mice, suggesting behavioural modifications were primarily driven by insoluble Aβ. Currently, aged *App*$^{NL\text{-}F}$ KI mice have not been tested for anxiety behaviours, but it would be interesting to see if as these mice age, and plaque pathology increases, whether their behavioural phenotype becomes more like the *App*$^{NL\text{-}G\text{-}F}$ KI genotype.

Several other AD mouse models exhibit impairments in social behaviour, including APP_{swe}/PS1 (Filali, et al., 2011) and Tg2576 mice (Deacon, et al., 2009). Latif-Hernandez et al. (2017) examined social behaviours in *App*$^{NL\text{-}G\text{-}F}$ KI mice and found that although not significant, the discrimination ratio for exploring a novel mouse compared to an empty cage, and for comparing between the previously explore mouse and a second novel mouse, had fallen to chance by 10 months of age (Latif-Hernandez, et al., 2017). We found that although *App*$^{NL\text{-}F}$ KI and *App*$^{NL\text{-}G\text{-}F}$ KI mice show robust preference for exploring a novel conspecific compared to an empty cage, social recognition discrimination was close to chance for both sexes. However, statistical analysis of the absolute times spent exploring each conspecific did not reveal a significant effect of genotype upon discrimination, suggesting that the overall detrimental effect upon social behaviour is likely to be mild. We did, however, find that social preference as measured by discriminating a social odour cue was only impaired in female *App*$^{NL\text{-}G\text{-}F}$ KI mice. A key difference between our study and Latif-Hernandez et al. (2017) is that they used only female mice. Our study, with mixed-sex groups, suggests that females show a greater impairment in social behaviour than males, which will be an important consideration for future studies.

The ACC and amygdala are brain regions well established with mediating anxiety/fear and social behaviours (Davidson, 2002,Davis, 1992,Davis, et al., 1994,Etkin, et al., 2011). Further, these areas are also susceptible to degeneration in early AD pathology (Huang, et al., 2002,Poulin, et al., 2011,Scheff and Price, 2001). Other transgenic AD mouse models, notably the APP/PS1 mouse, exhibit early amygdala pathology (Guo, et al., 2017,Lin, et al., 2015), whilst Aβ deposition in the PDAPP mouse begins in the cingulate cortex (Schenk, et al., 1999). Together, we hypothesised that structural and functional alterations within these regions could partly explain behavioural impairments.

Our analysis of microstructural integrity using DTI revealed that the prefrontal cortex of *App*$^{NL\text{-}G\text{-}F}$ KI mice, including the OFC and ACC, was substantially altered, and the functional consequences of these changes to the ACC was that gamma oscillations lost their dependency upon NMDA receptors, notably GluN2B receptors. Thus far, there have been limited investigations into the biological pathways altered in *App*$^{NL\text{-}G\text{-}F}$ KI mice. Using rsfMRI, Latif-Hernandez et al. (2017) found that the cingulate cortex was the most significantly altered brain region, with no visible impairment in the amygdala. Although further work is required to definitively describe the physiological pathways that explain the altered behaviour in *App*$^{NL\text{-}G\text{-}F}$ KI mice, our findings present an important step in this process. Although other brain regions likely contribute to changes in anxiety and social behaviours (gamma oscillations have also been found altered in the medial entorhinal cortex of *App*$^{NL\text{-}G\text{-}F}$ KI mice (Nakazono, et al., 2017)), the prefrontal cortex could represent a key region. Neural oscillations in the medial prefrontal cortex have clear links to anxiety behaviours, both in the open field and elevated plus maze (Adhikari, et al., 2010), and medial prefrontal cortex gamma is

required for the expression of social novelty (Cao, et al., 2018). Additionally, the loss of GluN2B or its phosphorylation impairs social behaviour (Jacobs, et al., 2015,Wang, et al., 2011) and increases anxiety in the open field (Hanson, et al., 2014) and the elevated plus maze (Delawary, et al., 2010). Furthermore, NMDA receptors are necessary for gamma mediated by the goblet cell interneurons within the entorhinal cortex (Middleton, et al., 2008), with specific antagonism of GluN2B significantly reducing hippocampal gamma power (Hanson, et al., 2013). Together, insoluble Aβ overexpression drives prefrontal cortical alterations through gamma oscillatory impairments by reduced GluN2B expression. The lack significant changes to gamma, gene expression and microstructure in the amygdala suggests that it may not undergo pathological damage at the same rate as other regions. This indicates that social and anxiety behavioural impairments in *App*$^{NL\text{-}G\text{-}F}$ KI mice are driven by regions that do not include the amygdala, although further work will be required to corroborate this.

Conclusion

The findings presented herein show a clear dichotomy of anxiety behaviours between two different paradigms. Contrasted to *App*$^{NL\text{-}F}$ KI mice, only *App*$^{NL\text{-}G\text{-}F}$ KI mice exhibited any change in anxiety behaviours, suggesting that plaque-based Aβ is responsible for these effects. We further postulate that microstructural integrity, gamma oscillatory function and *Grin2b* expression within the prefrontal cortex may, in part, explain these behavioural changes. Our data continues to highlight the importance of using AD models that do not have the confound of APP overexpression. Further studies will be required to continue to refine the mechanisms that explain anxiety impairments in *App*$^{NL\text{-}G\text{-}F}$ KI mice.

Figure Legends

Figure 1

Anxiety behaviours in 8 month old *App* KI mice in the open field and elevated plus maze. **A.** Given 30 minutes free ambulation, all genotypes expressed similar amounts of locomotor activity as quantified by distance travelled. **B.** $App^{NL\text{-}G\text{-}F}$ KI mice displayed thigmotaxis in the open field, spending significantly more time against the walls and less time in the centre zone (**C**). Conversely, $App^{NL\text{-}G\text{-}F}$ KI mice spent significantly more time exploring the open arms of the elevated plus maze (**D**) and significantly less time within the closed arms (**E**), suggesting an anxiolytic profile. ***=P<0.001, **=P<0.01, *=P<0.05. Error bars = s.e.m. Wild-type n = 21, $App^{NL\text{-}F}$ KI n = 19, $App^{NL\text{-}G\text{-}F}$ KI n = 19.

Figure 2

Social behaviours in *App* KI mice. **A.** All genotypes showed similar preference for exploring a novel, same-sexed novel conspecific (Stranger 1), compared to an empty cage. However, *App* KI mice displayed a weaker discrimination between the previously explored mouse (Stranger 1) and a second novel conspecific (Stranger 2), which differed by sex (**B**). To further investigate this sex difference, social recognition discrimination ratios were spilt by sex. Male (**C**) and female (**D**) *App* KI mice did not show discrimination that was significantly above chance, suggesting a social recognition impairment. Mice were then required to discriminate between a social smell (soiled bedding) or a non-social smell (clean bedding). Although all male genotypes showed preference for exploring the social cue (**E**), the discrimination ratio for female $App^{NL\text{-}G\text{-}F}$ KI mice was not above chance (**F**). ***=P<0.001,

**=P<0.01, *=P<0.05. Error bars = s.e.m. Wild-type: male n = 9, female n = 11; *App*$^{NL-F}$ KI: male n = 10, female n = 9; *App*$^{NL-G-F}$ KI: male n = 10, female n = 9.

Figure 3

Alterations in fractional anisotropy (FA) and mean diffusivity (MD) in the hippocampus. DTI images of the hippocampus was segmented at two regions; anterior (Bregma -1.94 mm) and posterior (Bregma -3.28 mm). FA was not significantly altered between the wild-type and *App*$^{NL-G-F}$ KI mice in the anterior (**A**) and posterior (**B**) hippocampus. MD of the anterior hippocampus did not differ between the genotypes (**C**), however MD in the posterior hippocampus was significantly higher in *App*$^{NL-G-F}$ KI mice (**D**). Diffusivity was further characterised by examining axial (AD) and radial (RD) diffusivity. AD was significantly increased in the anterior hippocampus of *App*$^{NL-G-F}$ KI mice (**E**), but not in the posterior hippocampus (**F**). RD did not differ between the genotypes in the anterior hippocampus, but *App*$^{NL-G-F}$ KI mice had significantly increased RD posterior hippocampus compared to wild-types. **=P<0.01, *=P<0.05. Error bars = s.e.m. Wild-type n = 8, *App*$^{NL-G-F}$ KI n = 8.

Figure 4

Alterations in fractional anisotropy (FA) and mean diffusivity (MD) in the orbitofrontal cortex and anterior cingulate cortex of the prefrontal cortex. DTI images were segmented for the orbitofrontal cortex at Bregma +2.58 mm and for the anterior cingulate cortex at Bregma +1.18 mm. FA was not significantly altered between the wild-type and *App*$^{NL-G-F}$ KI mice in the orbitofrontal cortex (**A**), however MD was significantly higher for *App*$^{NL-G-F}$ KI mice (**B**). Similarly, FA was did not differ between the genotypes for the anterior cingulate cortex (**C**), but MD was significantly higher in

App^{NL-G-F} KI mice (**D**). Axial (AD) and radial (RD) diffusivity was then analysed. In *App*$^{NL-G-F}$ KI mice, AD (**E**) and RD (**F**) were both significantly increased in the orbitofrontal cortex. AD (**G**) and RD (**H**) were also both increased in *App*$^{NL-G-F}$ KI mice in the anterior cingulate cortex. *=P<0.05. Error bars = s.e.m. Wild-type n = 8, *App*$^{NL-G-F}$ KI n = 8.

Figure 5

Gamma oscillations in the amygdala and anterior cingulate cortex. **A. i.** Pooled power spectrum of gamma oscillatory activity in the basolateral amygdala in WT (black) and *App*$^{NL-G-F}$ (blue) KI mice. **ii.** Example traces showing 500 ms of gamma oscillatory activity in WT (black) and *App*$^{NL-G-F}$ (blue) KI mice. Scale bar 50 mV. **iii.** Graph showing the effect of NMDA receptor antagonism (20 mM CPP) on the frequency of basolateral amygdala gamma oscillations. **iv.** Graph showing the effect of NMDA receptor antagonism (20 mM CPP) on the amplitude of basolateral amygdala gamma oscillations. **B. i.** Pooled power spectrum of gamma oscillatory activity in the anterior cingulate cortex in WT (black) and *App*$^{NL-G-F}$ (blue) KI mice. **ii.** Example traces showing 500 ms of gamma oscillatory activity in WT (black) and *App*$^{NL-G-F}$ (blue) KI mice. Scale bar 20 mV. **iii.** Graph showing the effect of NMDA receptor antagonism (20 mM CPP) on the frequency of anterior cingulate cortex gamma oscillations. **iv.** Graph showing the effect of NMDA receptor antagonism (20 mM CPP) on the amplitude of anterior cingulate cortex gamma oscillations. *=P<0.05. Error bars = s.e.m. Wild-type n = 5, *App*$^{NL-G-F}$ KI n = 5.

Figure 6.

Gene expression within the frontal cortex and amygdala. **A.** Although *App*$^{NL-G-F}$ KI mice generally had higher expression of our selected genes within the amygdala, these were not significantly different to wild-types. **B.** Within the frontal cortex, expression of both *Grin2b* and *Stxbp1* (Munc18-1) were significantly reduced in *App*$^{NL-G-F}$ KI mice. *=P<0.05. Error bars = s.e.m. Wild-type n = 6, *App*$^{NL-G-F}$ KI n = 6.

Table 1

Gene	Orientation	Sequence
Grin1	Forward	CCTACTCCCAACGACCACTT
	Reverse	AGACGCGCATCATCTCAAAC
Grin2a	Forward	TTGGGAGCGGGTACATCTTT
	Reverse	CTCCTGCCATGTTGTCGATG
Grin2b	Forward	GGAGAGGGTGGGAAAATGGA
	Reverse	CACTGAGAGGGTCCACACTT
Dlg4	Forward	TCAACAGTGTGGGGCTAGAG
	Reverse	TGCCCAAGTAGCTGCTATGA
Gapdh	Forward	CAACTCCCACTCTTCCACCT
	Reverse	GAGTTGGGATAGGGCCTCTC

References

Adhikari, A., Topiwala, M.A., Gordon, J.A. 2010. Synchronized activity between the ventral hippocampus and the medial prefrontal cortex during anxiety. Neuron 65(2), 257-69. doi:10.1016/j.neuron.2009.12.002.

Adolphs, R. 2010. What does the amygdala contribute to social cognition? Annals of the New York Academy of Sciences 1191, 42-61. doi:10.1111/j.1749-6632.2010.05445.x.

Bannerman, D.M., Rawlins, J.N., McHugh, S.B., Deacon, R.M., Yee, B.K., Bast, T., Zhang, W.N., Pothuizen, H.H., Feldon, J. 2004. Regional dissociations within the hippocampus--memory and anxiety. Neuroscience and biobehavioral reviews 28(3), 273-83. doi:10.1016/j.neubiorev.2004.03.004.

Bennett, D.A., Schneider, J.A., Tang, Y., Arnold, S.E., Wilson, R.S. 2006. The effect of social networks on the relation between Alzheimer's disease pathology and level of cognitive function in old people: a longitudinal cohort study. The Lancet Neurology 5(5), 406-12. doi:10.1016/S1474-4422(06)70417-3.

Bloom, G.S. 2014. Amyloid-beta and tau: the trigger and bullet in Alzheimer disease pathogenesis. JAMA neurology 71(4), 505-8. doi:10.1001/jamaneurol.2013.5847.

Buzsaki, G., Wang, X.J. 2012. Mechanisms of gamma oscillations. Annual review of neuroscience 35, 203-25. doi:10.1146/annurev-neuro-062111-150444.

Cao, W., Lin, S., Xia, Q.Q., Du, Y.L., Yang, Q., Zhang, M.Y., Lu, Y.Q., Xu, J., Duan, S.M., Xia, J., Feng, G., Xu, J., Luo, J.H. 2018. Gamma Oscillation Dysfunction in mPFC Leads to Social Deficits in Neuroligin 3 R451C Knockin Mice. Neuron 97(6), 1253-60 e7. doi:10.1016/j.neuron.2018.02.001.

Chung, J.A., Cummings, J.L. 2000. Neurobehavioral and neuropsychiatric symptoms in Alzheimer's disease: characteristics and treatment. Neurologic clinics 18(4), 829-46.

Dachtler, J., Glasper, J., Cohen, R.N., Ivorra, J.L., Swiffen, D.J., Jackson, A.J., Harte, M.K., Rodgers, R.J., Clapcote, S.J. 2014. Deletion of alpha-neurexin II results in autism-related behaviors in mice. Translational psychiatry 4, e484. doi:10.1038/tp.2014.123.

Davidson, R.J. 2002. Anxiety and affective style: role of prefrontal cortex and amygdala. Biological psychiatry 51(1), 68-80.

Davis, M. 1992. The role of the amygdala in fear and anxiety. Annual review of neuroscience 15, 353-75. doi:10.1146/annurev.ne.15.030192.002033.

Davis, M., Rainnie, D., Cassell, M. 1994. Neurotransmission in the rat amygdala related to fear and anxiety. Trends in neurosciences 17(5), 208-14.

Deacon, R.M., Koros, E., Bornemann, K.D., Rawlins, J.N. 2009. Aged Tg2576 mice are impaired on social memory and open field habituation tests. Behavioural brain research 197(2), 466-8. doi:10.1016/j.bbr.2008.09.042.

Delawary, M., Tezuka, T., Kiyama, Y., Yokoyama, K., Inoue, T., Hattori, S., Hashimoto, R., Umemori, H., Manabe, T., Yamamoto, T., Nakazawa, T. 2010. NMDAR2B tyrosine phosphorylation regulates anxiety-like behavior and CRF expression in the amygdala. Molecular brain 3, 37. doi:10.1186/1756-6606-3-37.

Driver, J.E., Racca, C., Cunningham, M.O., Towers, S.K., Davies, C.H., Whittington, M.A., LeBeau, F.E. 2007. Impairment of hippocampal gamma-frequency oscillations in vitro in mice overexpressing human amyloid precursor protein (APP). The European journal of neuroscience 26(5), 1280-8. doi:10.1111/j.1460-9568.2007.05705.x.

Etkin, A., Egner, T., Kalisch, R. 2011. Emotional processing in anterior cingulate and medial prefrontal cortex. Trends in cognitive sciences 15(2), 85-93. doi:10.1016/j.tics.2010.11.004.

Ferretti, L., McCurry, S.M., Logsdon, R., Gibbons, L., Teri, L. 2001. Anxiety and Alzheimer's disease. Journal of geriatric psychiatry and neurology 14(1), 52-8. doi:10.1177/089198870101400111.

Filali, M., Lalonde, R., Rivest, S. 2011. Anomalies in social behaviors and exploratory activities in an APPswe/PS1 mouse model of Alzheimer's disease. Physiology & behavior 104(5), 880-5. doi:10.1016/j.physbeh.2011.05.023.

Franklin, K., Paxinos, G. 2008. The Mouse Brain in Stereotaxic Coordinates. Academic Press.

Guo, C., Long, B., Hu, Y., Yuan, J., Gong, H., Li, X. 2017. Early-stage reduction of the dendritic complexity in basolateral amygdala of a transgenic mouse model of Alzheimer's disease. Biochemical and biophysical research communications 486(3), 679-85. doi:10.1016/j.bbrc.2017.03.094.

Hanson, J.E., Meilandt, W.J., Gogineni, A., Reynen, P., Herrington, J., Weimer, R.M., Scearce-Levie, K., Zhou, Q. 2014. Chronic GluN2B antagonism disrupts behavior in wild-type mice without protecting against synapse loss or memory impairment in Alzheimer's disease mouse models. The Journal of neuroscience : the official journal of the Society for Neuroscience 34(24), 8277-88. doi:10.1523/JNEUROSCI.5106-13.2014.

Hanson, J.E., Weber, M., Meilandt, W.J., Wu, T., Luu, T., Deng, L., Shamloo, M., Sheng, M., Scearce-Levie, K., Zhou, Q. 2013. GluN2B antagonism affects interneurons and leads to immediate and persistent changes in synaptic plasticity, oscillations, and behavior. Neuropsychopharmacology : official publication of the American College of Neuropsychopharmacology 38(7), 1221-33. doi:10.1038/npp.2013.19.

Hart, D.J., Craig, D., Compton, S.A., Critchlow, S., Kerrigan, B.M., McIlroy, S.P., Passmore, A.P. 2003. A retrospective study of the behavioural and psychological symptoms of mid and late phase Alzheimer's disease. International journal of geriatric psychiatry 18(11), 1037-42. doi:10.1002/gps.1013.

Hitti, F.L., Siegelbaum, S.A. 2014. The hippocampal CA2 region is essential for social memory. Nature 508(7494), 88-92. doi:10.1038/nature13028.

Huang, C., Wahlund, L.O., Svensson, L., Winblad, B., Julin, P. 2002. Cingulate cortex hypoperfusion predicts Alzheimer's disease in mild cognitive impairment. BMC neurology 2, 9.

Jacobs, S., Wei, W., Wang, D., Tsien, J.Z. 2015. Importance of the GluN2B carboxy-terminal domain for enhancement of social memories. Learning & memory 22(8), 401-10. doi:10.1101/lm.038521.115.

Jost, B.C., Grossberg, G.T. 1995. The natural history of Alzheimer's disease: a brain bank study. Journal of the American Geriatrics Society 43(11), 1248-55.

Klein, A.S., Donoso, J.R., Kempter, R., Schmitz, D., Beed, P. 2016. Early Cortical Changes in Gamma Oscillations in Alzheimer's Disease. Frontiers in systems neuroscience 10, 83. doi:10.3389/fnsys.2016.00083.

Kuiper, J.S., Zuidersma, M., Oude Voshaar, R.C., Zuidema, S.U., van den Heuvel, E.R., Stolk, R.P., Smidt, N. 2015. Social relationships and risk of dementia: A systematic review and meta-analysis of longitudinal cohort studies. Ageing research reviews 22, 39-57. doi:10.1016/j.arr.2015.04.006.

Lalonde, R., Lewis, T.L., Strazielle, C., Kim, H., Fukuchi, K. 2003. Transgenic mice expressing the betaAPP695SWE mutation: effects on exploratory activity, anxiety, and motor coordination. Brain research 977(1), 38-45.

Latif-Hernandez, A., Shah, D., Craessaerts, K., Saido, T., Saito, T., De Strooper, B., Van der Linden, A., D'Hooge, R. 2017. Subtle behavioral changes and increased prefrontal-

hippocampal network synchronicity in APP(NL-G-F) mice before prominent plaque deposition. Behavioural brain research. doi:10.1016/j.bbr.2017.11.017.

Lin, T.W., Shih, Y.H., Chen, S.J., Lien, C.H., Chang, C.Y., Huang, T.Y., Chen, S.H., Jen, C.J., Kuo, Y.M. 2015. Running exercise delays neurodegeneration in amygdala and hippocampus of Alzheimer's disease (APP/PS1) transgenic mice. Neurobiology of learning and memory 118, 189-97. doi:10.1016/j.nlm.2014.12.005.

Livingston, G., Sommerlad, A., Orgeta, V., Costafreda, S.G., Huntley, J., Ames, D., Ballard, C., Banerjee, S., Burns, A., Cohen-Mansfield, J., Cooper, C., Fox, N., Gitlin, L.N., Howard, R., Kales, H.C., Larson, E.B., Ritchie, K., Rockwood, K., Sampson, E.L., Samus, Q., Schneider, L.S., Selbaek, G., Teri, L., Mukadam, N. 2017. Dementia prevention, intervention, and care. Lancet 390(10113), 2673-734. doi:10.1016/S0140-6736(17)31363-6.

Ly, P.T., Cai, F., Song, W. 2011. Detection of neuritic plaques in Alzheimer's disease mouse model. Journal of visualized experiments : JoVE (53). doi:10.3791/2831.

McHugh, S.B., Deacon, R.M., Rawlins, J.N., Bannerman, D.M. 2004. Amygdala and ventral hippocampus contribute differentially to mechanisms of fear and anxiety. Behavioral neuroscience 118(1), 63-78. doi:10.1037/0735-7044.118.1.63.

McNally, J.M., McCarley, R.W., McKenna, J.T., Yanagawa, Y., Brown, R.E. 2011. Complex receptor mediation of acute ketamine application on in vitro gamma oscillations in mouse prefrontal cortex: modeling gamma band oscillation abnormalities in schizophrenia. Neuroscience 199, 51-63. doi:10.1016/j.neuroscience.2011.10.015.

Middleton, S., Jalics, J., Kispersky, T., Lebeau, F.E., Roopun, A.K., Kopell, N.J., Whittington, M.A., Cunningham, M.O. 2008. NMDA receptor-dependent switching between different gamma rhythm-generating microcircuits in entorhinal cortex. Proceedings of the National Academy of Sciences of the United States of America 105(47), 18572-7. doi:10.1073/pnas.0809302105.

Moy, S.S., Nadler, J.J., Perez, A., Barbaro, R.P., Johns, J.M., Magnuson, T.R., Piven, J., Crawley, J.N. 2004. Sociability and preference for social novelty in five inbred strains: an approach to assess autistic-like behavior in mice. Genes, brain, and behavior 3(5), 287-302. doi:10.1111/j.1601-1848.2004.00076.x.

Nadler, J.J., Moy, S.S., Dold, G., Trang, D., Simmons, N., Perez, A., Young, N.B., Barbaro, R.P., Piven, J., Magnuson, T.R., Crawley, J.N. 2004. Automated apparatus for quantitation of social approach behaviors in mice. Genes, brain, and behavior 3(5), 303-14. doi:10.1111/j.1601-183X.2004.00071.x.

Nakazono, T., Lam, T.N., Patel, A.Y., Kitazawa, M., Saito, T., Saido, T.C., Igarashi, K.M. 2017. Impaired In Vivo Gamma Oscillations in the Medial Entorhinal Cortex of Knock-in Alzheimer Model. Frontiers in systems neuroscience 11, 48. doi:10.3389/fnsys.2017.00048.

Okuyama, T., Kitamura, T., Roy, D.S., Itohara, S., Tonegawa, S. 2016. Ventral CA1 neurons store social memory. Science 353(6307), 1536-41. doi:10.1126/science.aaf7003.

Palmer, K., Berger, A.K., Monastero, R., Winblad, B., Backman, L., Fratiglioni, L. 2007. Predictors of progression from mild cognitive impairment to Alzheimer disease. Neurology 68(19), 1596-602. doi:10.1212/01.wnl.0000260968.92345.3f.

Pervolaraki, E., Dachtler, J., Anderson, R.A., Holden, A.V. 2017. Ventricular myocardium development and the role of connexins in the human fetal heart. Scientific reports 7(1), 12272. doi:10.1038/s41598-017-11129-9.

Pervolaraki, E., Dachtler, J., Anderson, R.A., Holden, A.V. 2018. The developmental transcriptome of the human heart. Scientific reports 8(1), 15362. doi:10.1038/s41598-018-33837-6.

Pervolaraki, E., Tyson, A.L., Pibiri, F., Poulter, S.L., Reichelt, A.C., Rodgers, R.J., Clapcote, S.J., Lever, C., Andreae, L.C., Dachtler, J. 2018. The within-subject application of diffusion tensor MRI and CLARITY reveals brain structural changes in Nrxn2 deletion mice. bioRxiv. doi:10.1101/300806.

Poulin, S.P., Dautoff, R., Morris, J.C., Barrett, L.F., Dickerson, B.C., Alzheimer's Disease Neuroimaging, I. 2011. Amygdala atrophy is prominent in early Alzheimer's disease and relates to symptom severity. Psychiatry research 194(1), 7-13. doi:10.1016/j.pscychresns.2011.06.014.

Saito, T., Matsuba, Y., Mihira, N., Takano, J., Nilsson, P., Itohara, S., Iwata, N., Saido, T.C. 2014. Single App knock-in mouse models of Alzheimer's disease. Nature neuroscience 17(5), 661-3. doi:10.1038/nn.3697.

Sakakibara, Y., Sekiya, M., Saito, T., Saido, T.C., Iijima, K.M. 2018. Cognitive and emotional alterations in App knock-in mouse models of Abeta amyloidosis. BMC neuroscience 19(1), 46. doi:10.1186/s12868-018-0446-8.

Scheff, S.W., Price, D.A. 2001. Alzheimer's disease-related synapse loss in the cingulate cortex. Journal of Alzheimer's disease : JAD 3(5), 495-505.

Scheltens, P., Blennow, K., Breteler, M.M., de Strooper, B., Frisoni, G.B., Salloway, S., Van der Flier, W.M. 2016. Alzheimer's disease. Lancet 388(10043), 505-17. doi:10.1016/S0140-6736(15)01124-1.

Schenk, D., Barbour, R., Dunn, W., Gordon, G., Grajeda, H., Guido, T., Hu, K., Huang, J., Johnson-Wood, K., Khan, K., Kholodenko, D., Lee, M., Liao, Z., Lieberburg, I., Motter, R., Mutter, L., Soriano, F., Shopp, G., Vasquez, N., Vandevert, C., Walker, S., Wogulis, M., Yednock, T., Games, D., Seubert, P. 1999. Immunization with amyloid-beta attenuates Alzheimer-disease-like pathology in the PDAPP mouse. Nature 400(6740), 173-7. doi:10.1038/22124.

Shin, L.M., Liberzon, I. 2010. The neurocircuitry of fear, stress, and anxiety disorders. Neuropsychopharmacology : official publication of the American College of Neuropsychopharmacology 35(1), 169-91. doi:10.1038/npp.2009.83.

Simon, A.M., Schiapparelli, L., Salazar-Colocho, P., Cuadrado-Tejedor, M., Escribano, L., Lopez de Maturana, R., Del Rio, J., Perez-Mediavilla, A., Frechilla, D. 2009. Overexpression of wild-type human APP in mice causes cognitive deficits and pathological features unrelated to Abeta levels. Neurobiology of disease 33(3), 369-78. doi:10.1016/j.nbd.2008.11.005.

Teri, L., Ferretti, L.E., Gibbons, L.E., Logsdon, R.G., McCurry, S.M., Kukull, W.A., McCormick, W.C., Bowen, J.D., Larson, E.B. 1999. Anxiety of Alzheimer's disease: prevalence, and comorbidity. The journals of gerontology Series A, Biological sciences and medical sciences 54(7), M348-52.

Wang, C.C., Held, R.G., Chang, S.C., Yang, L., Delpire, E., Ghosh, A., Hall, B.J. 2011. A critical role for GluN2B-containing NMDA receptors in cortical development and function. Neuron 72(5), 789-805. doi:10.1016/j.neuron.2011.09.023.

Whyte, L.S., Hemsley, K.M., Lau, A.A., Hassiotis, S., Saito, T., Saido, T.C., Hopwood, J.J., Sargeant, T.J. 2018. Reduction in open field activity in the absence of memory deficits in the App(NL-G-F) knock-in mouse model of Alzheimer's disease. Behavioural brain research 336, 177-81. doi:10.1016/j.bbr.2017.09.006.

Wilson, R.S., Krueger, K.R., Arnold, S.E., Schneider, J.A., Kelly, J.F., Barnes, L.L., Tang, Y., Bennett, D.A. 2007. Loneliness and risk of Alzheimer disease. Archives of general psychiatry 64(2), 234-40. doi:10.1001/archpsyc.64.2.234.

Figure 1

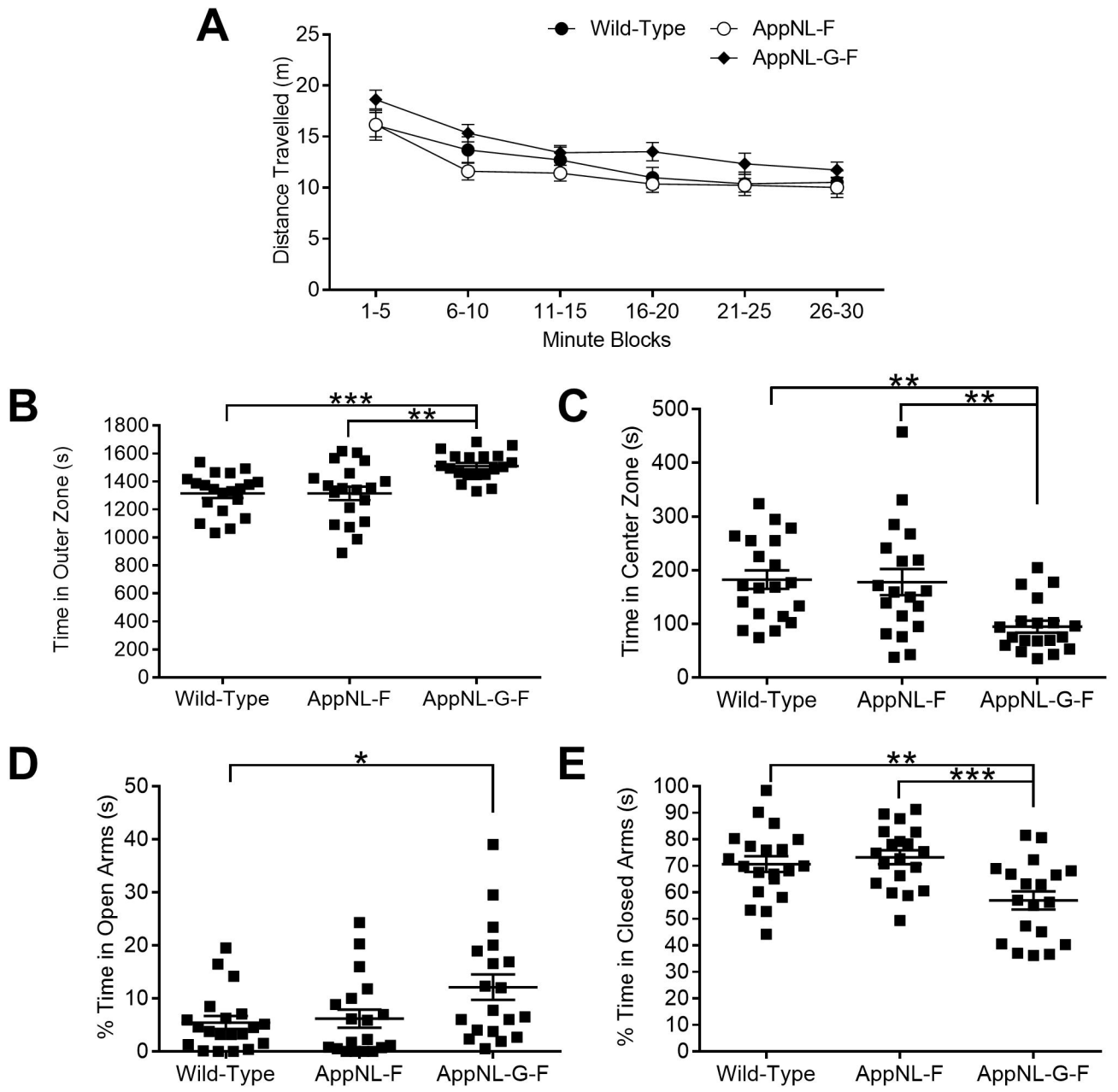
A
Wild-Type
AppNL-F
AppNL-G-F
Distance Travelled (m)
0
5
10
15
20
25
1-5
6-10
11-15
16-20
21-25
26-30
Minute Blocks
B
Time in Outer Zone (s)
0
200
400
600
800
1000
1200
1400
1600
1800
***
**
Wild-Type
AppNL-F
AppNL-G-F
C
Time in Center Zone (s)
0
100
200
300
400
500
**
**
Wild-Type
AppNL-F
AppNL-G-F
D
% Time in Open Arms (s)
0
10
20
30
40
50
*
Wild-Type
AppNL-F
AppNL-G-F
E
% Time in Closed Arms (s)
0
10
20
30
40
50
60
70
80
90
100
**
***
Wild-Type
AppNL-F
AppNL-G-F

Figure 2

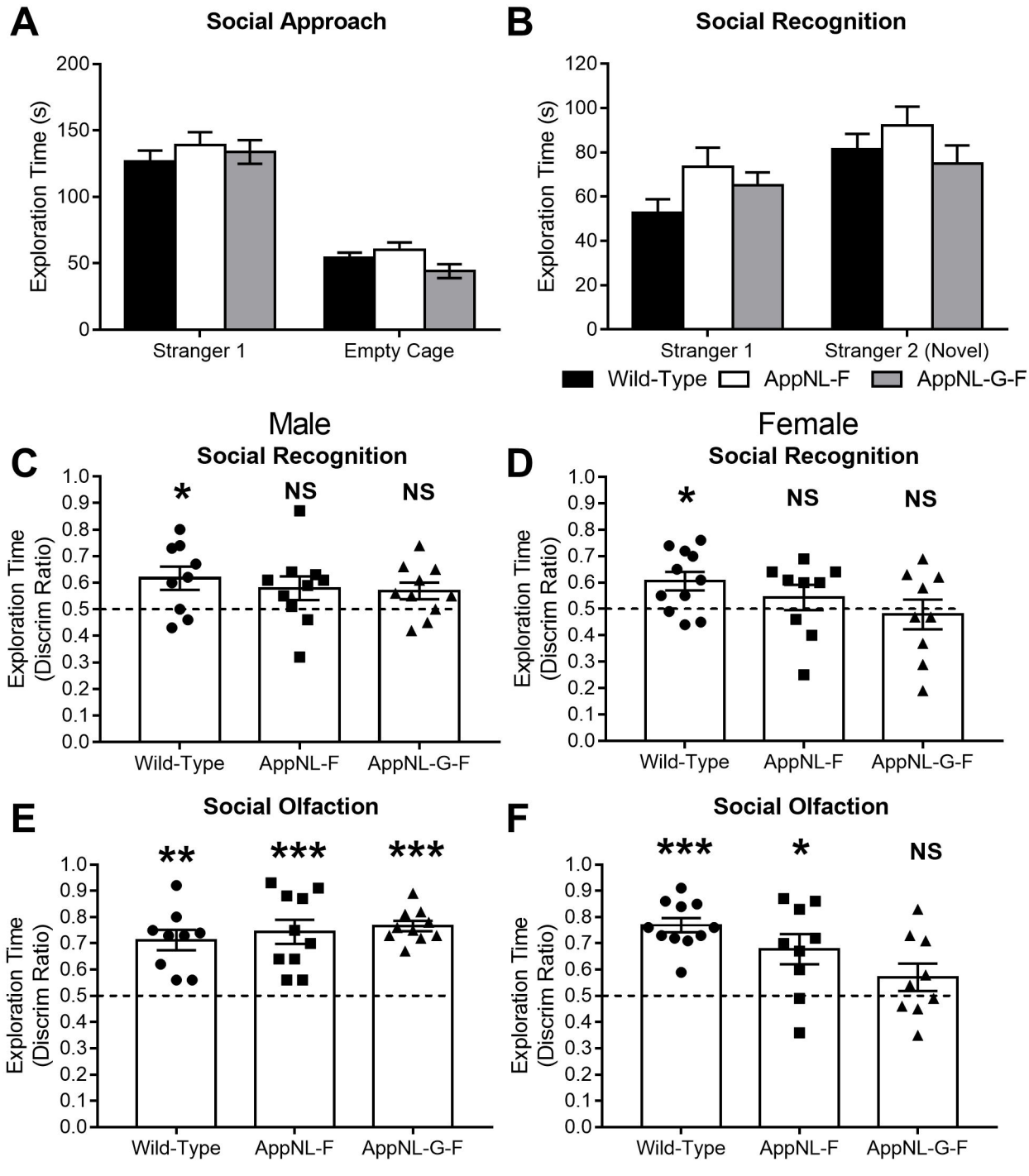
A
Social Approach
Exploration Time (s)
200
150
100
50
0
Stranger 1
Empty Cage
B
Social Recognition
Exploration Time (s)
120
100
80
60
40
20
0
Stranger 1
Stranger 2 (Novel)
Wild-Type
AppNL-F
AppNL-G-F
Male
Female
C
Social Recognition
D
Social Recognition
Exploration Time (Discrim Ratio)
1.0
0.9
0.8
0.7
0.6
0.5
0.4
0.3
0.2
0.1
0.0
*
NS
NS
Wild-Type
AppNL-F
AppNL-G-F
E
Social Olfaction
F
Social Olfaction
**
***
***
*
NS

Figure 3

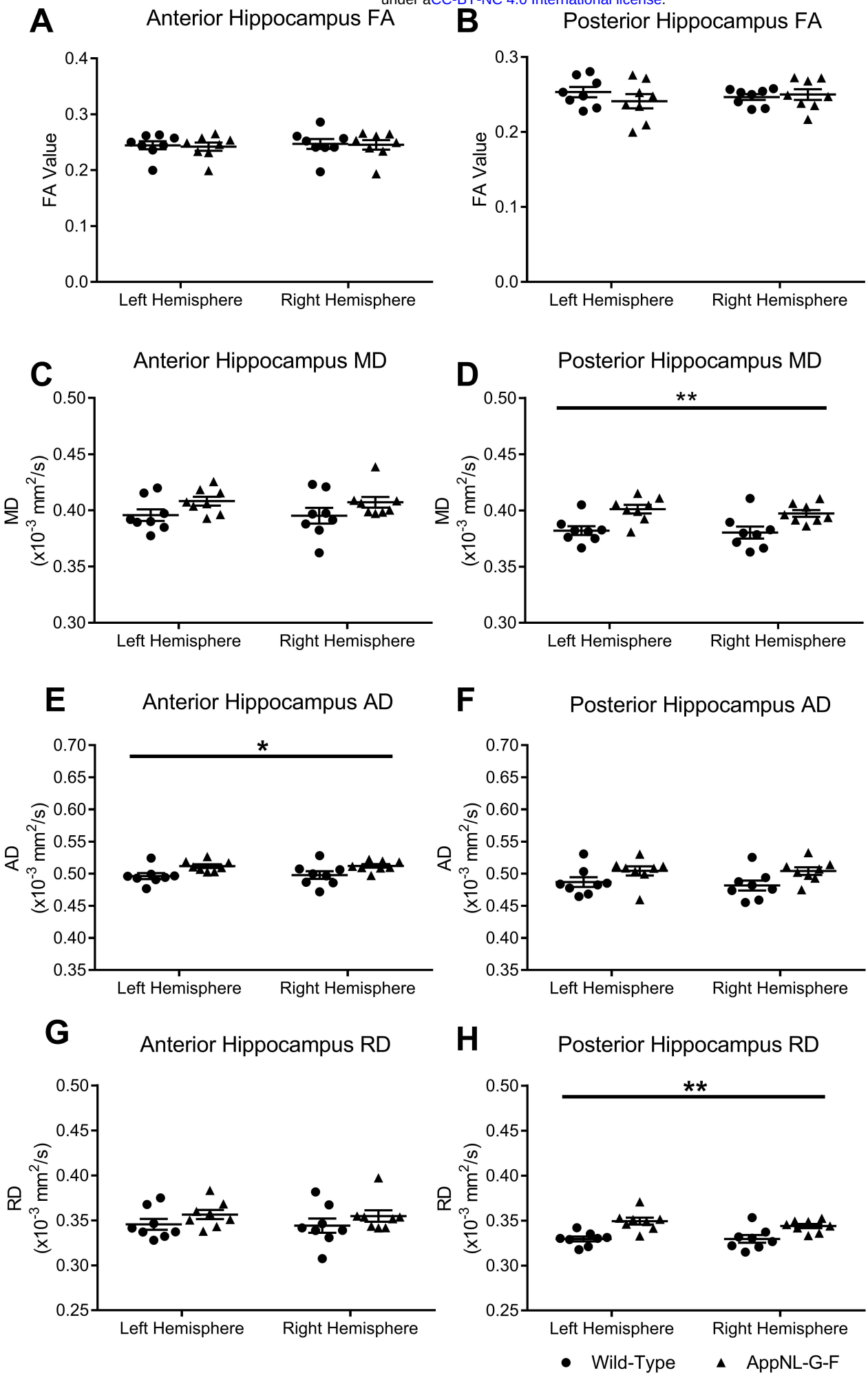

Figure 4

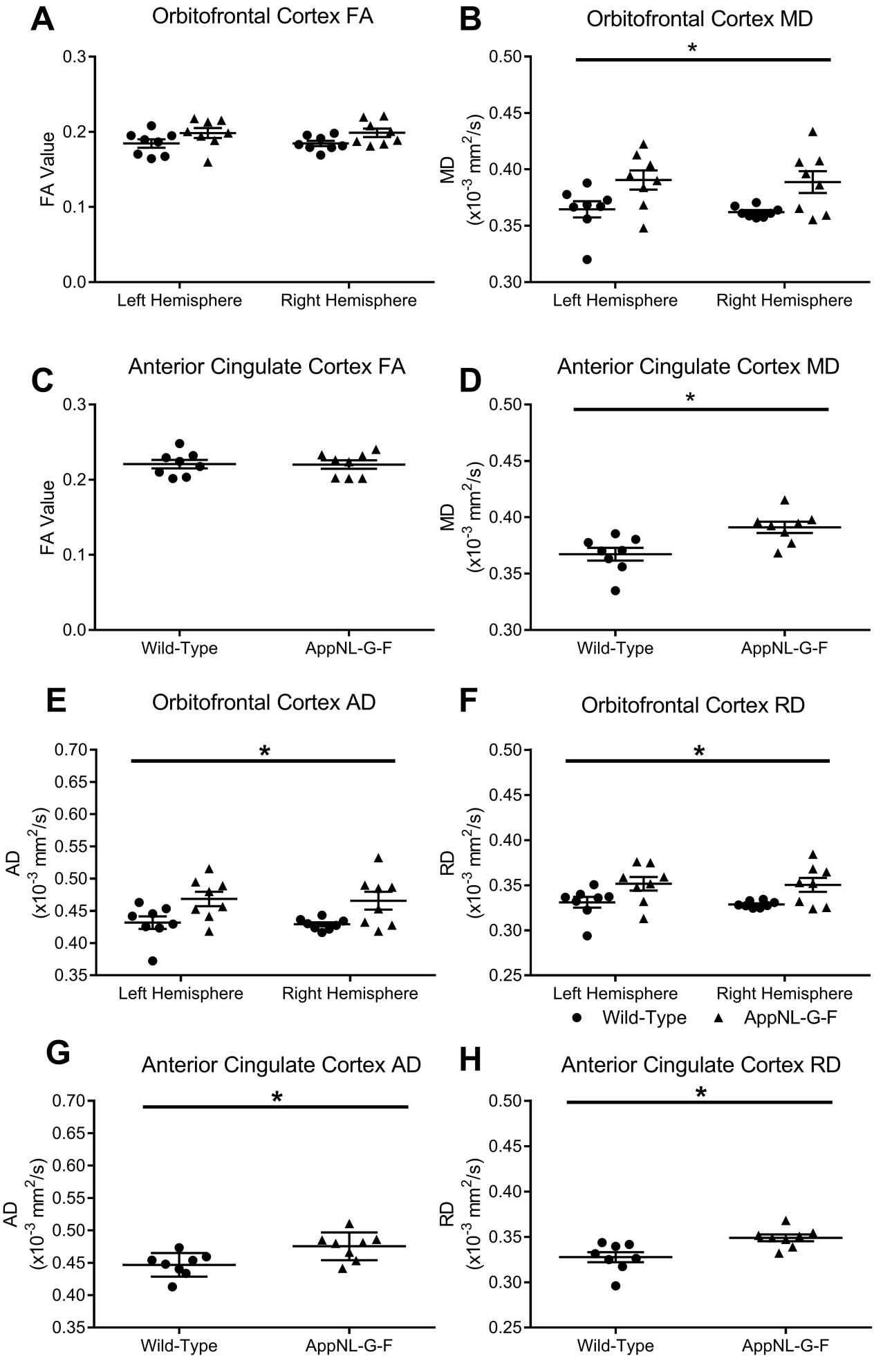

Figure 5

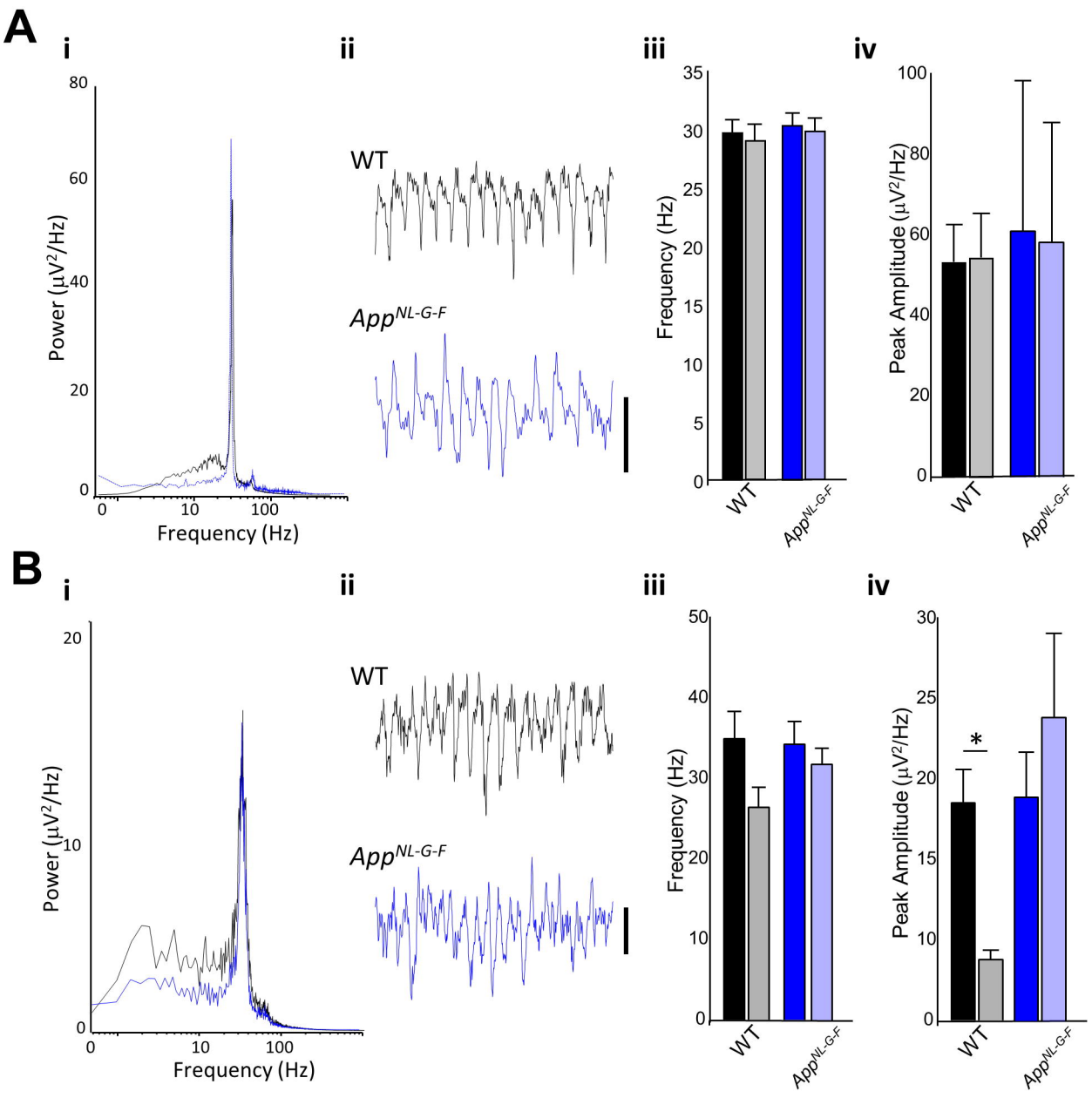
A
i
ii
iii
iv
Power (μV²/Hz)
Frequency (Hz)
WT
App^NL-G-F
Frequency (Hz)
Peak Amplitude (μV²/Hz)
B
i
ii
iii
iv
Power (μV²/Hz)
Frequency (Hz)
WT
App^NL-G-F
Frequency (Hz)
Peak Amplitude (μV²/Hz)
*

Figure 6

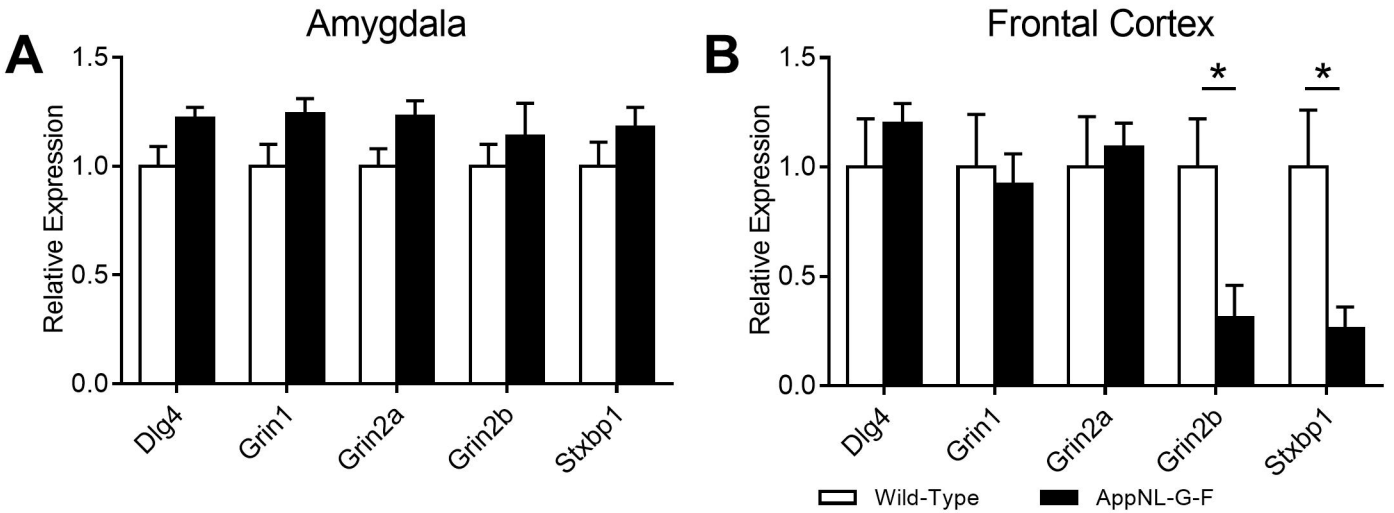
A
Amygdala
Relative Expression
1.5
1.0
0.5
0.0
Dlg4
Grin1
Grin2a
Grin2b
Stxbp1
B
Frontal Cortex
Relative Expression
1.5
1.0
0.5
0.0
*
*
Dlg4
Grin1
Grin2a
Grin2b
Stxbp1
Wild-Type
AppNL-G-F